PREDICTING MECHANICAL BEHAVIOR OF 3D PRINTED STRUCTURES USING MECHANICS OF COMPOSITES AND FRACTURE

by

MEGHA TANGRI

Presented to the Faculty of the Graduate School of

The University of Texas at Arlington in Partial Fulfillment

of the Requirements

for the Degree of

MASTER OF SCIENCE IN MECHANICAL ENGINEERING

THE UNIVERSITY OF TEXAS AT ARLINGTON

May 2018

Acknowledgements

I am grateful and highly obliged to my supervisor, *Dr. Ashfaq Adnan* for his continuous and indispensable guidance and motivation throughout the research. It was an honor to have him as my mentor.

I thank *Dr. Wendy Shen* and *Dr. Robert Taylor* for being on my committee and sparing their precious time for reviewing my work and suggesting ways of improvement.

I feel obliged to M*r. Amit Khatri* for sharing his experience and research data to be used as reference. I also extend my thanks to *Stratasys America Makes* for partially funding this project.

I would like to thank *Mr. Kermit Beird* and *Mr. Sam* for all their indispensable help, encouragement, skills and expertise. I thank them for allowing me to use the resources of UTA MAE Machine Shop.

A heartfelt gratitude to late *Dr. Wen S. Chan* for taking courses Fundamentals of Composites and Advanced Components, thereby equipping us with knowledge and motivation to pursue this research work.

I thank all the *MMPL lab mates, Ms Rajni Chahal, Mr Fuad Hassan, Mr Khandakar Abu Hasan Mahmud, Mr Riaz Kayser, Mr Ishak Khan, Mr Saket Thapliyal, Mr Blesson Isaac* and *Mr Krutarth Patel* for their support and encouragement throughout the journey.

April 27, 2018

Abstract

PREDICTING MECHANICAL BEHAVIOR OF 3D PRINTED STRUCTURES USING MECHANICS OF COMPSITES AND FRACTURE

Megha Tangri, MS

The University of Texas at Arlington, 2018

Supervising Professor: Ashfaq Adnan

Recently, additive manufacturing, or 3D printing as it is more commonly called, has taken a big leap in the manufacturing industry. This technology is rapidly moving from prototyping to manufacturing using metals, polymers, concrete and even composites. Unlike subtractive methods of manufacturing, additive manufacturing can be used to manufacture parts with highly directional mechanical properties.

This research focuses on predicting tensile failure of 3D printed polymer structures in different raster orientations using composites lamination theory. Previously it was found experimentally that tensile strengths of 3D printed specimens decrease when raster orientations changes from 0° to 90°. The proposed model developed confirms the experimental trends observed for ULTEM 9085. The samples comprise of 14 laminae with varying volumes of 0° and 90° raster orientation. It is discussed how geometry of a printed structure creates a difference in strength variation of 3D printed structures. It is also found that stacking sequence affects failure strength. Finite Element Analysis has been conducted to compare the analytical and experimental studies to find a co-relation of failure force corresponding to the first ply failure of the laminate samples.

The latter part of the research explores the fracture and flexure strengths of the ABS resin. Experiment was designed to manufacture number of straight bar specimens with variation in initial crack length and size, and specimen thickness to study the behavior of crack growth. The experiments helped establish a co-relation between bending and fracture energies and how they varied with thickness and crack length of specimens.

Table of Contents

List of Illustrations

List of Tables

Chapter 1

Introduction

Additive manufacturing or 3D printing, as it is commonly called, is one of the fastest growing technologies. It has been used a lot for rapid prototyping and now is finding its place in the manufacturing industry. The technology is being widely used or being considered in space applications, aerospace and automotive industry, medical and healthcare industry, ceramic industry and now 3D printers are used for hobby ideas at homes too [1-10]. Additive manufacturing can be done using polymers, composites, metals and even ceramics.

Polymers are long chains of repetitive units of carbon compounds. They are used to make plastics. They are also used in composites industry. Thermoplastics are the kinds of plastics that can be molded and remolded. They have a high strength to weight ratio. The most common plastics used for 3D printing are ABS (Acrylonitrile Butadiene Styrene) and PLA (Polylactic Acid). ULTEM 9085 is a very popular material in the automotive and aerospace industry because of its high chemical and thermal resistance. It is a high performing Fused Deposition Modeling (FDM) thermoplastic. It has a high strength to weight ratio and flame, smoke, toxicity (FST) ratings.

Composites are made from two or more materials. These materials have different material properties. Fiber reinforced composites are the most widely used type of composites where strong fibers such as carbon, glass etc are reinforced in polymer matrix. Depending on fiber orientations, directional properties in composites can also be

achieved. To control directional properties consistently, unidirectional or orthotropic laminae are stacked together to form a laminate.

Composites Lamination Theory (CLT) is used extensively to predict failure for composite laminates. One of the objectives of this research is to investigate the application of CLT to failure prediction of 3D printed polymer structures. The major motivation to carry out this research came from the resembling microstructural features of polymers and fiber reinforced composites.

Majorly, the fiber properties define the directional properties of the composite materials. In 3D printing too, the raster orientation of the extruded print plays a significant role in defining the directional properties of the print. In this research, the stacking sequences of laminae in a composite laminate has been hypothesized to be analogous to the fiber reinforced polymer extruded for 3D printing.

The scope of this research is to predict failure of the 3D printed structures out of ULTEM 9085 using Classical Lamination theory of composites. The first ply failure load is also predicted using the Finite Element Analysis. The research also includes studying the crack propagation in various 3D printed samples of ABS.

1.1 Fused Deposition Modeling

Fused deposition modelling (FDM) or fused filament fabrication (FFF) is one of the techniques of additive manufacturing. It uses a heated filament which is deposited layer by layer over a pre-heated bed of a 3D printer to fabricate a part. FDM is a very

popular technique. Previous studies have shown that FDM can be used to fabricate parts with specific directional properties.

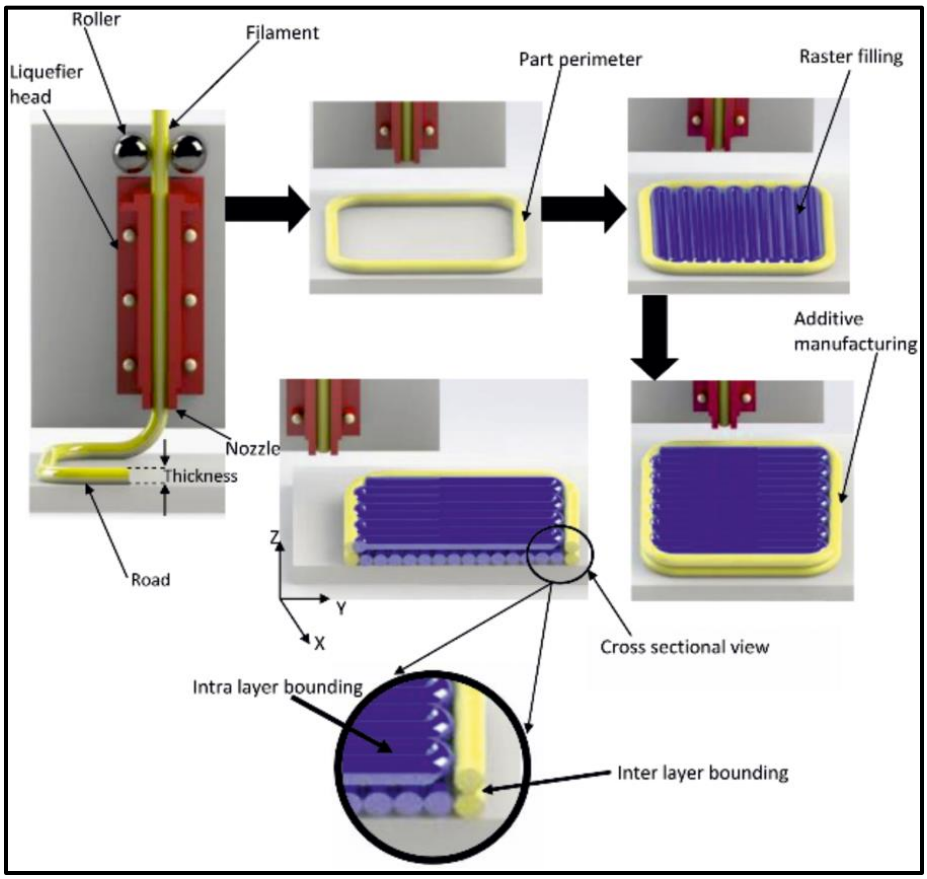

Figure 1-1 Fused Deposition Modeling (FDM) [12]

Sung-Hoon Ahn *et al* [13] compares the mechanical behavior of ABS specimens manufactured using injection molding with those manufactured using fused deposition (FDM) technique. The authors establish that the air gap and raster orientation affect the mechanical properties of the FDM printed parts. They also go on to show that the additively manufactured parts possess anisotropic properties.

Anna Bellini *et al* [14] studies the mechanical characterization of additively manufactured ABS parts. The authors establish that the mechanical properties of the final parts depend on the raster orientation, and the chosen path or the way the every layer is filled by roads.

The effect of layer parameters on additively manufactured ABS plastics were studied at the South Dakota State University. The study shows that there is a linear rate of increase of maximum force required to break a specimen when the number of layers in the laminate is increased. The elastic modulus as well as the maximum stress also increased with the number of layers until 12 layers. However, the rate of increase in the elastic modulus and the maximum stress slowed as the layers were increased after 12 layers [16].

1.2 Application of Classical Lamination Theory

There have been many studies in the past that have predicted failure of 3D printed parts using various analytical approaches. In this study, the analytical prediction of the mechanical behavior of FDM printed parts using composites' Classical Lamination Theory (CLT) has been studied.

A technical memorandum of NASA [17] set up a research program to work on the strain-based micromechanics model that would incorporate the classical lamination theory to analyze the multilayered and symmetric laminates of polymer matrix composites under in-plane loading. Poisson effect was also incorporated into the micromechanics model.

Zou *et al* [18] compared the isotropic model of FDM printed parts with the anisotropic model. The authors established the mechanical properties for both the cases. However, the authors suggested using the anisotropic model for better precision.

Casavola *et al* [19] studied the orthotropic mechanical behavior of FDM printed parts using classical lamination theory. The mechanical properties were first derived experimentally. The results were verified by experiments. The study also went on to show that the mean UTS of ABS and PLA varied by 74.3% and 55.2% respectively as the raster orientation was varied from 0° to 90°.

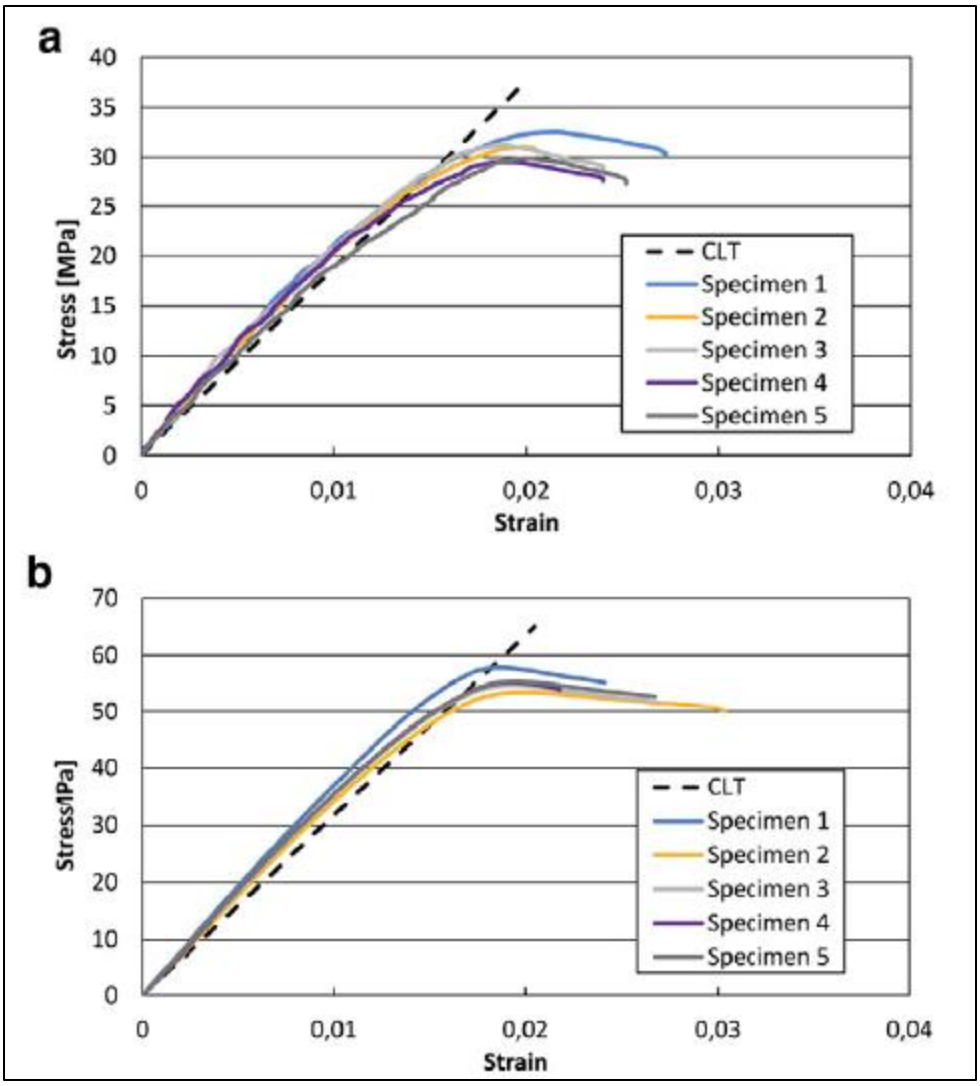

Figure 1-2 Stress Strain comparisons of Experimental data vs CLT for ABS (a) and PLA (b) [16]

Bertoldi *et al* [20] also showed a similar approach towards obtaining stiffness matrices which can be applied using CLT. The approach involved calculating the compliance matrices using the experimentally developed orthotropic mechanical

properties. The authors stated that the study can be used for computational analyses which involves CLT model.

Magalhães *et al* [21] studied the effect of deposition strategies on mechanical behavior of FDM printed parts. The tensile and bending experiment results determined the stiffness and strength of the specimens with each layer oriented at a different raster angle. The classical lamination theory model was used to predict the stiffness of the specimens. However, it was established by the authors that the model was not accurate to predict the experimentally studied mechanical behavior and they go on to suggest the use of a better analytical model.

Alaimo *et al* [22] showed the effect of fiber orientation, filament dimensions and chemical composition on mechanical behavior of additively manufactured ABS samples. The study went on to establish that CLT model can predict the macroscale in-plane stiffness at the macroscale. The authors experimentally investigated the effect of meso-structure on the macroscale mechanical properties.

1.3 Fracture Tests

There have been several studies done in the past to examine the mode I interlaminar fracture for FDM printed parts. The DCB tests conducted in these studies [23-26] used modified specimens and standards to obtain the fracture toughness and stress intensity factor.

Patel *et al* [27] studied the fracture behavior of FDM printed ABS samples experimentally as well as using numerical methods. The authors followed the D5045 ASTM standard for the shape and size of the samples. They established that on increasing the initial crack length, the maximum load required for fracture of the samples decreases.

Park *et al* [28] proposed an estimate of the strength of lattice structures manufactured using FDM by considering interlaminar fracture. For finding out the mode I interlaminar fracture toughness, the authors used ASTM D5528-13 standard for unidirectional fiber reinforced polymer matrix composites as the basis and they called it peel test. However, the authors used modified DCB specimen to create a small area where only two deposition paths are bonded. For embedding an initial crack in the specimen, the fabrication process was paused at the 7^{th} layer, a 23mm long strap of a 3M blue paper masking tape was applied and then the fabrication process was resumed. After the peel tests, Cohesive Zone Model (CZM) was used for numerical modelling in which the authors calibrate the cohesive parameters based on the peel test results. Then they went on to propose a simulation model which predicts the initial crack length. The authors noted that their proposed CZM approach was able to capture mode I fracture and improve the accuracy of the strength-estimation procedure.

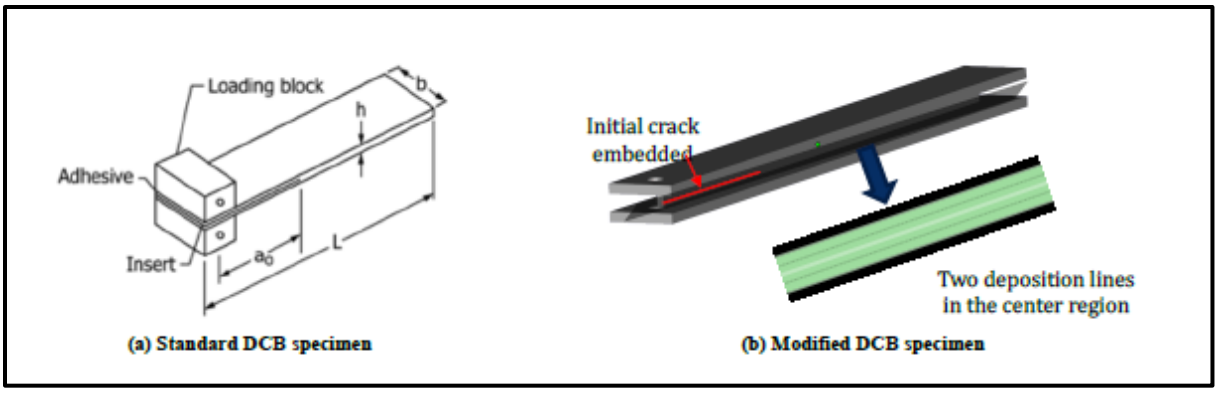

Figure 1-3 Standard and Modified DCB specimen [28]

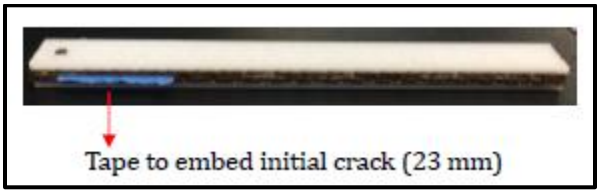

Figure 1-4 Modified DCB specimen for Peel Test [28]

Spoerk *et al* [29] conducted the DCB test to study inter-layer cohesion of the PLA samples for various layer thickness. For the experiments for mode I interlaminar fracture, the authors used multiple steps to machine the fabricated specimens for creating an initial crack: grooving, drilling and finally, using a wedge-shaped blade. They used the ASTM D5528 [30] standard for the DCB test and maintain a thickness of 12.25mm for all the specimens irrespective of the layer thickness. The authors noted challenges in preparation of some specimens. Also, due to failure of some specimens at the load line rather than delamination, some data could not be collected.

In this study, the specimens are modified as well. However, instead of embedding the initial crack, the initial crack was machined after the fabrication had been completed by FDM. The machining was accomplished using saw blades.

Chapter 2

Analytical Study

2.1 Introduction

The classical lamination theory is widely used to predict in-plane laminar stresses and strains of composite structures under mechanical, thermal and hygroscopic loads.

Model Assumptions

- All samples are considered to be failed vial fiber failure. Hence, the first fiber failure (FFF) is considered as the ultimate laminate failure (ULF).
- The mid-plane curvature is assumed to be zero. Hence, no bending is possible.

2.2 Deriving CLT for Analytical Study

Finding extensional stiffness, extensional - bending coupling and bending stiffness matrices -

$$[A] = \sum_{k=1}^{n} \bar{Q}\, t_{ply} \frac{lb}{in} \quad \text{———————} \ (1)$$

$$[B] = \frac{1}{2}\sum_{k=1}^{n} \bar{Q}\,(h_k^2 - h_{k-1}^2)\ \text{lb} \quad \text{———————} \ (2)$$

$$[D] = \frac{1}{3}\sum_{k=1}^{n} \bar{Q}\,(h_k^3 - h_{k-1}^3)\ \text{lb} - \text{in} \quad \text{———————} \ (3)$$

$[A], [B], [D]$ are axial, coupling and bending stiffnesses. t_{ply} is the thickness of each ply (=0.005m)

$$\begin{bmatrix}\bar{N}\\ \bar{M}\end{bmatrix} = \begin{bmatrix}A & B\\ B & D\end{bmatrix}\begin{bmatrix}\varepsilon^o\\ \kappa\end{bmatrix} \quad \text{———————} (4)$$

As there is no thermal or hygroscopic applied load, and no moment is applied either, we get from equation (4).

$$\begin{bmatrix}N\\ 0\end{bmatrix} = \begin{bmatrix}A & B\\ B & D\end{bmatrix}\begin{bmatrix}\varepsilon^o\\ \kappa\end{bmatrix} \quad \text{———————} (5)$$

$$\begin{bmatrix}\varepsilon^o\\ \kappa\end{bmatrix} = \begin{bmatrix}a & b\\ b^T & d\end{bmatrix}\begin{bmatrix}N\\ 0\end{bmatrix} \quad \text{———————} (6)$$

$$where \begin{bmatrix}a & b\\ b^T & d\end{bmatrix} = \begin{bmatrix}A & B\\ B & D\end{bmatrix}^{-1}$$

We know that the laminate is only under tensile loading. Considering, $\kappa = 0$, finding mid-plane strains,

$$\begin{bmatrix}\varepsilon_x^o\\ \varepsilon_y^o\\ \gamma_{xy}^o\end{bmatrix} = \begin{bmatrix}a_{11} & a_{12} & a_{13}\\ a_{21} & a_{22} & a_{23}\\ a_{31} & a_{32} & a_{33}\end{bmatrix}\begin{bmatrix}N_x\\ 0\\ 0\end{bmatrix} \quad \text{———————} (7)$$

Or,

$$[\varepsilon^o] = \begin{bmatrix}\varepsilon_x^o\\ \varepsilon_y^o\\ \gamma_{xy}^o\end{bmatrix} = \begin{bmatrix}a_{11}\\ a_{21}\\ a_{31}\end{bmatrix} N_x \quad \text{———————} (8)$$

Equation for strains developed at each ply is,

$$[\varepsilon]_{x-y}^k = [\varepsilon^o] + h_k[\kappa] \quad \text{———————} (9)$$

where, h_k is the distance of the ply from the mid-plane of the laminate.

Again considering,

$$\kappa = 0$$

$$\Rightarrow [\varepsilon]_{x-y}^k = [\varepsilon^o] \quad \text{———————} (10)$$

From equation (10), the strains developed in all plies are equal to the mid-plane strain.

Calculating stress developed in all plies:

$$[\sigma]_{x-y}^{k} = [\bar{Q}(\theta)]^{k}[\varepsilon]_{x-y}^{k}$$

$$by\,(10), [\sigma]_{x-y}^{k} = [\bar{Q}(\theta)]^{k}[\varepsilon^{o}] \quad \text{———————} (11)$$

$$[\sigma]_{x-y}^{k} = [\bar{Q}(\theta)]^{k}\begin{bmatrix} a_{11} \\ a_{21} \\ a_{31} \end{bmatrix} N_x \quad \text{———————} (12)$$

In principal material co-ordinates,

$$[\sigma]_{1-2}^{k} = [T_{\sigma}(\theta)][\sigma]_{x-y}^{k} \quad \text{———————} (13)$$

$$[\sigma]_{1-2}^{k} = [T_{\sigma}(\theta)][\bar{Q}(\theta)]^{k}\begin{bmatrix} a_{11} \\ a_{21} \\ a_{31} \end{bmatrix} N_x \quad \text{———————} (14)$$

By maximum stress failure criterion, failure occurs if any stress component exceeds the corresponding stress allowable. Failure will occur if,

$$\sigma_1^k \geq \begin{cases} F_{1t}, \sigma_1^k > 0 \\ -F_{1c}, \sigma_1^k < 0 \end{cases} \quad \text{———————} (15)$$

$$\sigma_2^k \geq \begin{cases} F_{2t}, \sigma_2^k > 0 \\ -F_{2c}, \sigma_2^k < 0 \end{cases} \quad \text{———————} (16)$$

$$\tau_{12}^k \geq F_6 \quad \text{———————} (17)$$

where F_{1t} and F_{1c} are stress allowables for tensile and compression respectively in 1 direction, F_{2t} and F_{2c} are stress allowables for tensile and compression respectively in 2 direction, and F_6 is the stress allowable in the $1-2$ direction, or shear direction.

To find the first ply failure load, say N_x^1 the stresses are equated to their corresponding allowable. The least magnitude of all the loads, becomes our first ply failure, or N_x^1.

As N_x is tensile and hence, is always positive, it does not affect the sign (and nature) of the stress found using equation (14).

Observations

It is noted that identical angle plies fail together in this case as the stress developed is independent of h_k.

As there are two types of angle plies, $0^o \ and \ 90^o$, at second ply failure the whole laminate fails.

It is hypothesized and later proved that under the application of only tensile load the first ply failure occurs at the 90^o plies due to matrix failure, and 0^o plies fail due to fiber failure.

Second Ply Failure (SPF) and First Fiber Failure (FFF)

After finding the first ply failure load, N_x^1 two changes were made –

The stress allowable changes after the first ply failure. The new allowables, with respect to each ply were found out by the following steps.

Step 1: Stresses developed in each ply due to the first ply failure (FPF) load N_x^1 were calculated.

Step 2: Corresponding original stress allowables ($F_{1t}, F_{1c}, F_{2t}, F_{2c}$, F_6) were then subtracted from the stresses calculated in Step 1.

This gave the new corresponding stress allowables, and they were unique for each ply as they depend on the ply's position..

For the second ply failure or other progressive failure load, the corresponding stress allowable with the latest alteration is used.

The material parameters are altered keeping in mind where the failure occurred. This will change the reduced stiffness matrix of the ply(ies) where the first ply failure had occurred. The failed plies are not removed as they still add to the stiffness. The process is defined by the following steps.

Step 1: Identify, r_1, r_2 and r_{12}.

fiber failure: $r_1 = r_2 = r_{12} = 0$

matrix failure: $r_1 = 1,\ r_2 = r_{12} = 0.25$

shear failure: $r_1 = 1,\ r_2 = r_{12} = 0.25$

Step 2:

$$E_1^* = r_1 E_1$$

$$E_2^* = r_2 E_2$$

$$G_{12}^* = r_{12} G_{12}$$

$$\upsilon_{12}^* = r_1 \upsilon_{12}$$

Step 3: $\bar{Q}(\theta)^*$ is calculated for all the plies which failed at N_x^1.

Step 4: A, B and D matrices are re-calculated.

After this, the second ply failure load, N_x^2, which is also the first fiber failure load is computed by repeating the same steps.

The ULF for our case is given by,

$$ULF = \frac{\sum_{i=1}^{n} N_x^i}{laminate\ thickness}$$

Or,

$$ULF = \frac{N_x^1 + N_x^2}{laminate\ thickness} \quad \text{———————} (18)$$

2.3 Results

The analytical study was carried out for different ply orientations of the tensile straight bar coupons. The chart below shows the Ultimate Tensile Strength of the 3D printed ULTEM 9085 straight bar coupons with varying number or volume of 90° (or transversely) oriented plies. This plot was generated from the tensile test experiment results which were a part of a previous study [1].

Using the Classical Lamination Theory, for each case of 0/90 plies orientation, all the permutations were considered to obtain the progressive failure load and the corresponding failure stress. The results are recorded as shown in the following tables. It was noted that the Ultimate Failure Stress was same if the first ply was oriented as 90° or the last ply was oriented as 90°, and the trend followed for other cases as well. Alternatively, if the defined CLT model is used, then the Ultimate Stress Failure will be same for any two cases if:

1. They have the same volume of 0/90 plies

2. In both the cases the 0/90 plies are present at same distance from the mid-plane

The analytical study also showed that as the volume of 90° plies increases, the deviation of the analytically modelled results from the experimental data increases.

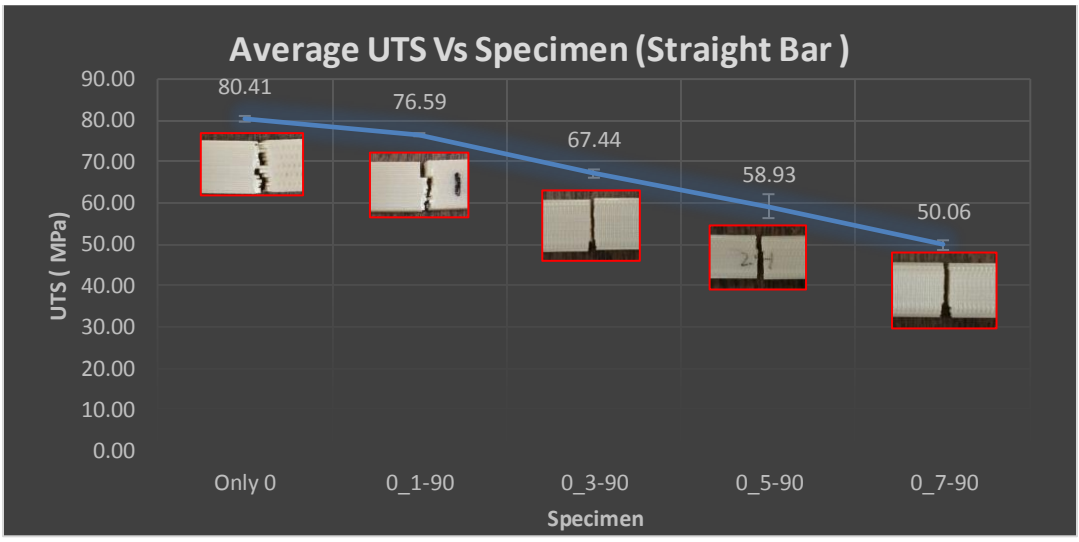

Figure 2-1 Experimental Tensile Test Results of ULTEM 9085 Straight Bar coupons

Table 2-1 1 ply 90°

Position of 90	UTS (MPa)	Experimental UTS (MPa)	Position of 90
1	75.91	76.59	14
2	76.11		13
3	76.26		12
4	76.37		11
5	76.45		10
6	76.50		9
7	76.52		8

Table 2-2 3 plies 90°

Position of 90	UTS (MPa)	Experimental UTS (MPa)	Position of 90
1,3,5	65.78	67.44	10,12,14
2,4,6	67.15		9,11,13
3,5,7	68.00		8,10,12
5,7,9	68.75		6,8,10

Table 2-3 5 plies 90°

Position of 90	UTS (MPa)	Experimental UTS (MPa)	Position of 90
1,3,5,7,9	58.44	58.93	6,8,10,12,14
2,4,6,8,10	60.18		5,7,9,11,13
3,5,7,9,11	60.95		4,6,8,10,12

Table 2-4 7plies 90°

Position of 90	UTS (MPa)	Experimental UTS (MPa)	Position of 90
1,3,5,7,9,11,13	53.06	50.06	2,4,6,8,10,12,14

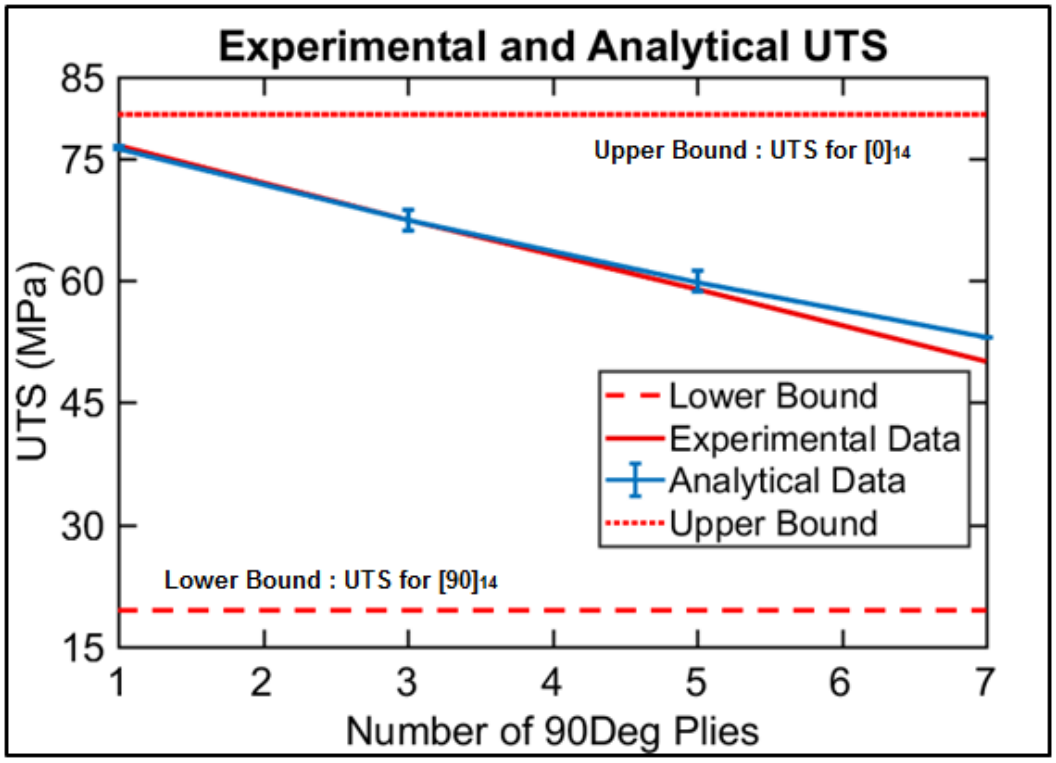

Figure 2-2 Experimental and Analytical Results

CLT was proved to be most accurate for layups with more 0° plies. The deviation of the analytical results from the experimental increases as the volume of 90° plies increase.

The maximum deviation of the analytical results from the experimental data was only 6% for the case of 50% volume of 90° and 0° i.e. 7 plies out of 14 oriented in the 90° direction.

This same analytical model based on Classical Lamination Theory was used to predict failure for other configurations also which were not tested experimentally. The following tables and graph give the results.

Table 2-5 2 plies 90°

Position of 90	UTS(MPa)	Position of 90
1,3	70.72	12,14
2,4	71.47	11,13
3,5	71.98	10,12
4,6	72.32	9,11
5,7	72.54	8,10
6,8	72.64	7,9

Table 2-6 4 plies 90°

Position of 90	UTS (MPa)	Position of 90
1,3,5,7	61.68	8,10,12,14
2,4,6,8	63.43	7,9,11,13
3,5,7,9	64.41	6,8,10,12
4,6,8,10	64.85	5,7,9,11

Table 2-7 6 plies 90°

Position of 90	UTS (MPa)	Position of 90
1,3,5,7,9,11	55.74	4,6,8,10,12,14
2,4,6,8,10,12	57.02	3,5,7,9,11,13

Table 2-8 8 plies 90°

Position of 0	UTS(MPa)	Position of 0
1,3,5,7,9,11	47.36	4,6,8,10,12,14
2,4,6,8,10,12	49.2	3,5,7,9,11,13

Table 2-9 9 plies 90°

Position of 0	UTS MPa)	Position of 0
1,3,5,7,9	41.14	6,8,10,12,14
2,4,6,8,10	43.66	5,7,9,11,13
3,5,7,9,11	45.35	4,6,8,10,12

Table 2-10 10 plies 90°

Position of 0	UTS (MPa)	Position of 0
1,3,5,7	36.04	8,10,12,14
2,4,6,8	38.05	7,9,11,13
3,5,7,9	40.11	6,8,10,12
5,7,9,11	41.53	4, 6,8,10

Table 2-11 11 plies 90°

Position of 0	UTS (MPa)	Position of 0
1,3,5	32.56	10,12,14
2,4,6	33.8	9,11,13
3,5,7	35.26	8,10,12
5,7,9	36.74	6,8,10

Table 2-12 12 plies 90°

Position of 0	UTS(MPa)	Position of 0
1,3	30.29	12,14
2,4	30.95	11,13
3,5	31.73	10,12
4,6	32.6	9,11
5,7	33.43	8,10
6,8	33.95	7,9

Table 2-12 13 plies 90°

Position of 0	UTS (MPa)	Position of 0
1	28.56	14
2	28.83	13
3	29.13	12
4	29.45	11
5	29.76	10
6	30.01	9
7	30.16	8

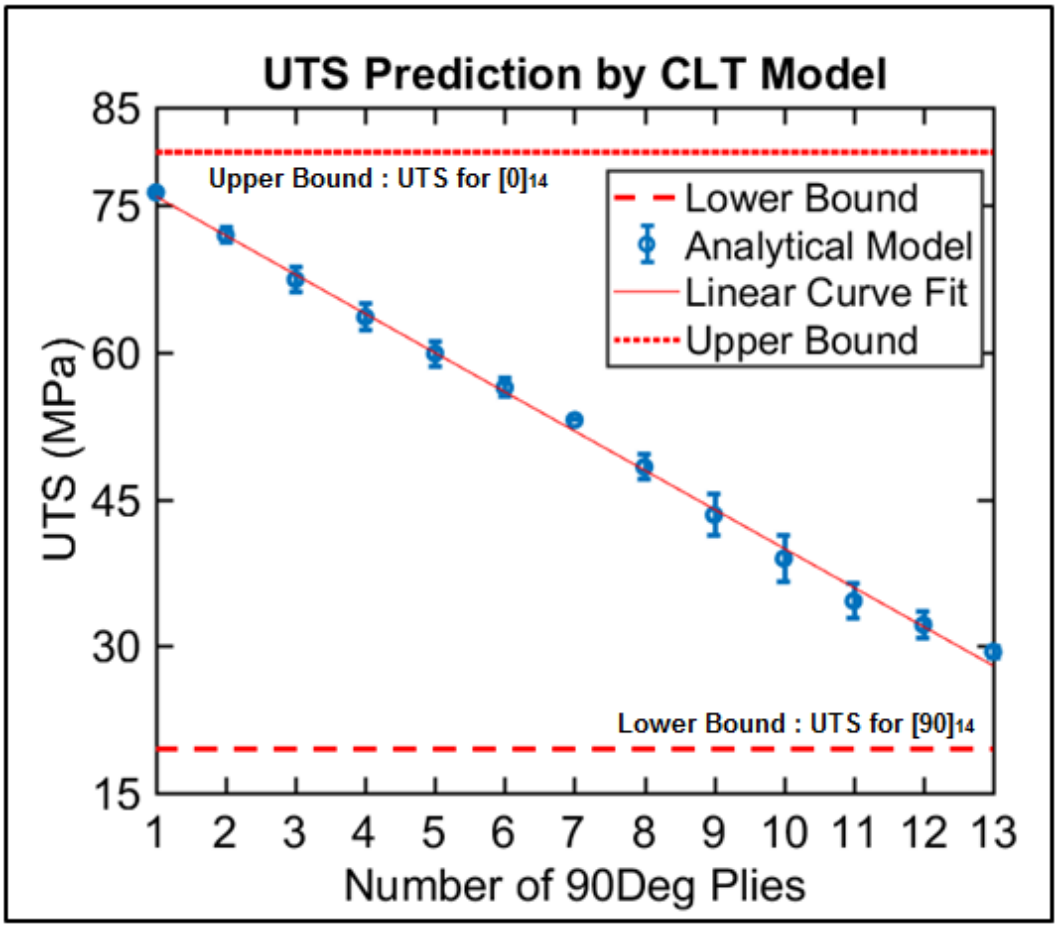

Figure 2-3 UTS Prediction using CLT Model

for varying number of 90° plies in the laminate from none to 14

It was observed that as the number of 90° plies increased from one to thirteen, the tensile strength decreases. This deviation is gradual and follows a linear trend. The upper bound represents the UTS for all 0° plies and the lower bound represents the UTS for all 90° plies. These values were derived experimentally. The UTS for all these cases are bound within the region defined by the UTS for all 0° oriented plies and all 90° oriented plies. However, the jump in the UTS values from thirteen plies 90° to all plies

oriented in 90° is not so gradual. Similarly, the jump from all 0° plies to one 90° ply is also not gradual. This behavior is assumed to occur due to fabrication defects such as voids and bonding between different layers.

Chapter 3

Computational Study

Computational study was performed after analytical studies to further understand the mechanical behavior of the ULTEM 9085 laminates under tensile load. This exercise helped analyze the transition between the linear and non-linear region of the experimentally obtained stress vs strain curves as shown in the figure 3-2.

The Dassault Systeme's ABAQUS software was used for static analysis of the composite laminates.

3.1 Methodology

Part Module

The part module is used to create part geometry in ABAQUS. It has a feature-based representation. It also gives the option to import geometry from other CAD software like, SolidWorks and CATIA. The part module was used to generate the CAD model of the straight bar coupon.

Property Module

The property module is used to define a wide range of characteristics of the geometry and material. This includes assigning material properties, defining material calibrations, defining sections, and defining composite layups.

The mechanical elastic lamina properties of ULTEM 9085 were defined as:

E_1 = 2480 MPa, E_2 = 1500 MPa, v = 0.3, $G_{12} = G_{13}$ = 160 MPa, G_{23} = 120 MPa

ABAQUS allows us to choose from three kinds of composite layup options: conventional shell, continuum shell, and solid. A conventional shell gives the option to assign different orientation and different material to the plies in the layup. A continuum shell also lets to assign different orientations and materials to the plies but it is generally used in modelling slender structures. Generally, these two options are used. The solid composite layup is used for the cases when transverse shear effects predominate, the normal stresses cannot be ignored or when accurate interlaminar stresses need to be visualized.

For this case, conventional shell model of composite layup was defined. All the plies had the same thickness. The orientations of plies were changed according to each case.

Step Module

In the step module, the 'Static, General' step is created.

Load Module

In the Load Module, the boundary conditions are established on the geometry. Two nodes were created, one at the top and the other at the bottom, as shown. The bottom node was kept at ENCASTRE boundary condition, and tensile load was applied on the upper node.

Figure 3-1 Part modelling in Abaqus

3.2 Results

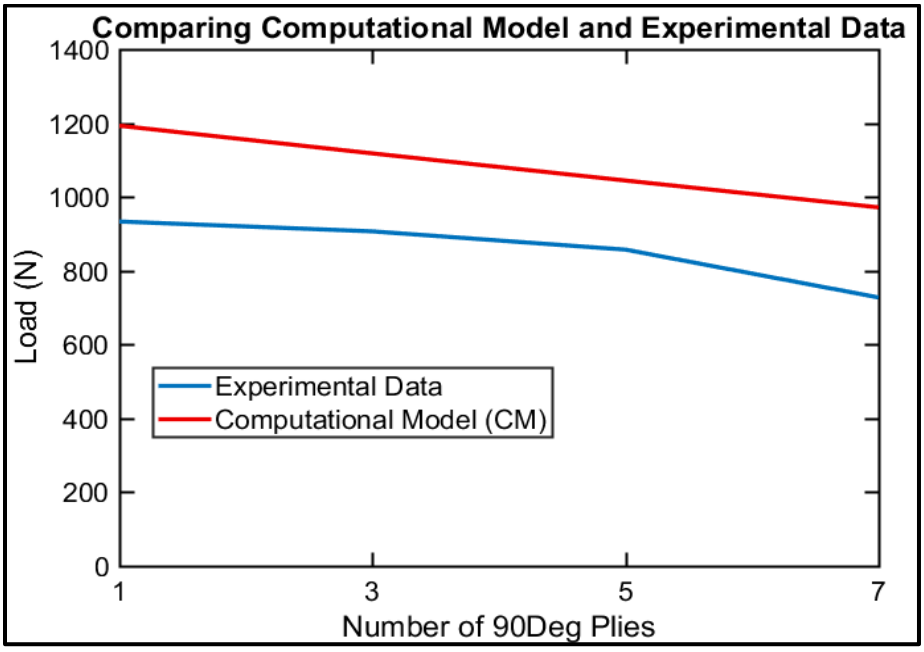

Figure 3-2 Computational Model and Experimental Data

against Number of 90° plies indicating similar behavior

It was noted that the experimental and computational curves ran almost parallel to each other. It was hypothesized that by the use of a correction factor calculated by dividing computationally obtained load by experimentally obtained load, the experimental data can be mapped. The correction factor was calculated to be 0.79.

The computational study did not account for the factors such as voids and gaps that might have been introduced while fabricating the specimens using FDM. The presence of voids tends to fail the structures at stress lower than the estimated [28]. This justifies the use of the correction factor. The computational study hence led to perform fracture tests to understand the mechanical behavior of the specimens more clearly. The fracture study has been presented in the following chapter.

Chapter 4

Experimental Study

4.2 Testing Standards and Procedures

Fracture Testing

Experiments were performed to analyze crack growth in specimens printed out of ABS plastic. For fracture analysis, the Double Cantilever Beam experiment was performed. The primary objective of the DCB test is to find the fracture toughness for mode I interlaminar fracture failure. The ASTM standardized test D5528 [30] was used as a reference to study fracture in this research. The reason for choosing this testing procedure was that the ABS specimens were manufactured by fused deposition modelling (FDM) and so the specimens possess anisotropic properties similar to unidirectional composites.

The recommended dimensions used for the DCB test were 125mm by 25mm by 5mm as recommended by the ASTM standard D5528-13. However, this study was performed on specimens with two different thicknesses, 5mm and 10mm, and with different initial crack length and size.

For successfully studying the crack propagation using the DCB test, the bending rigidity of the specimen should be high such that fracture occurs only through crack growth and not by bending. The Young's modulus in the fiber direction of the commonly used unidirectional fiber reinforced composites can vary from 39 GPa for E-Glass

composites to 294 GPa for Graphite epoxy composites [31]. However, the Young's modulus of ABS filament is 1.4 – 3.1 GPa [32]. Doubling the thickness of the specimens to 10mm increases the flexural rigidity by eight times.

The initial crack length was machined using saw blades. The tables below show the sample size of the experiments. The initial plan was to study the crack propagation in the specimens with four crack types (table 4-2). However, out of eight probable case, only four cases could be studied due to fabrication limitations.

The initial intention for creating the initial crack was at the interface of the two layers of the FDM fabricated specimens. However, due to the machining limitations pertaining to the size of the saw blades, the initial crack might have been developed inside the material for some specimens.

Table 4-1 Thicknesses chosen

Thickness (mm)	
5	10

Table 4-2 Initial crack dimensions

Crack Type	a_0 (mm)	Dia (mm)
A	12.06	0.25
B	12.06	0.76
C	50.8	0.25
D	50.8	0.76

Table 4-3 Probable Case Studies

Probable Case Studies			
5A	5B	5C	5D
10A	10B	10C	10D

Table 4-4 Case Studies Conducted

Case Studies Conducted			
5A	10A	10B	10D

4.3 Modelling and Fabrication of Specimens

The specimens were modelled using SolidWorks. The specimens were straight bar coupons with dimensions 125mm by 25mm and thickness of either 10mm or 5mm. The STL file created was sliced using Kisslicer v1.6.4.PolyPrinter 229 was used for 3D printing in XYZ raster orientation. The infill was kept at a 100%, the force path angle was maintained at 0° for all layers and the specimens were printed with a brim support of radius 5mm to avoid warping. The CAD model for 10mm thick sample has been shown in figure 4-2.

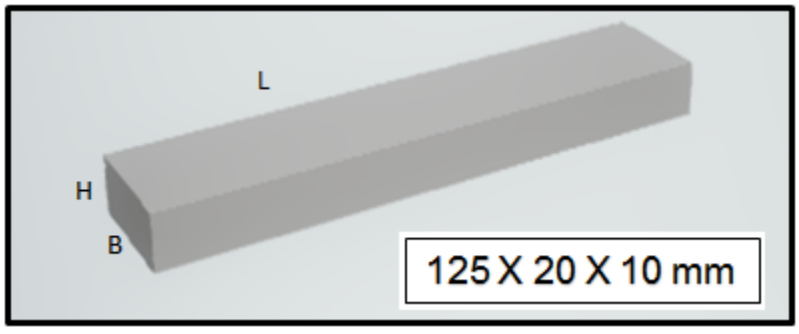

Figure 4-2 CAD Model

(a) w/o any support yielding bad sample

(b) w/ brim yielding desired sample

Figure 4-3 3D Printed Specimen of thickness 10mm

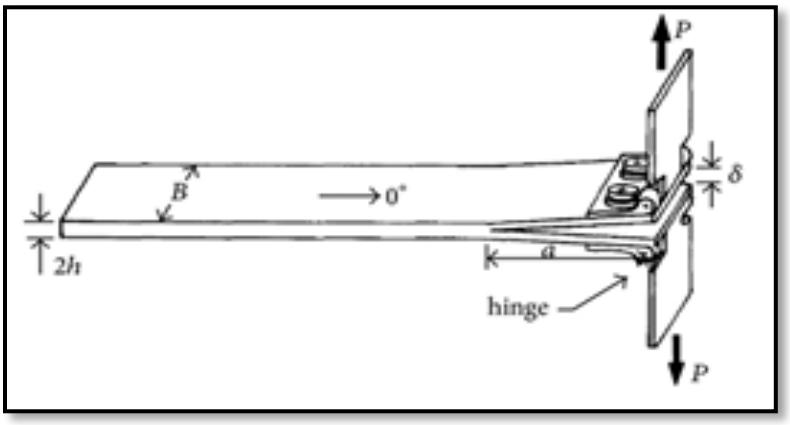

Figure 4-4 Sample with hinges placed [33]

The hinges used were made of acrylic plastic and they had steel rod of an eighth of an inch holding the piano hinges together, as shown in the figure.

For the specimens of type 10A, the hinges broke at higher loads due to their brittle nature. Metallic hinges would have performed better for this case.

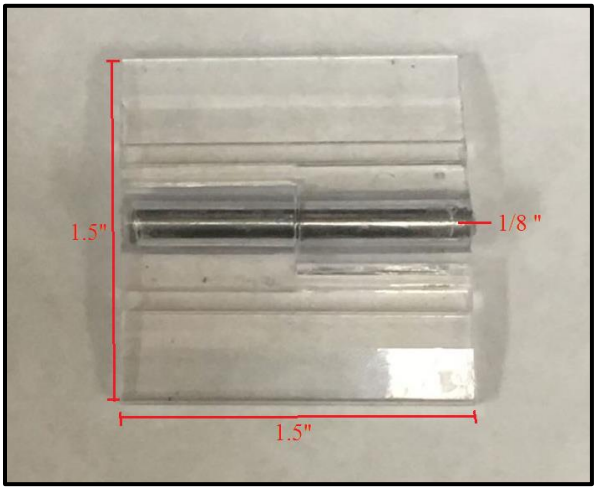

Figure 4-1 Acrylic Hinges used for DCB

4.4 Observations

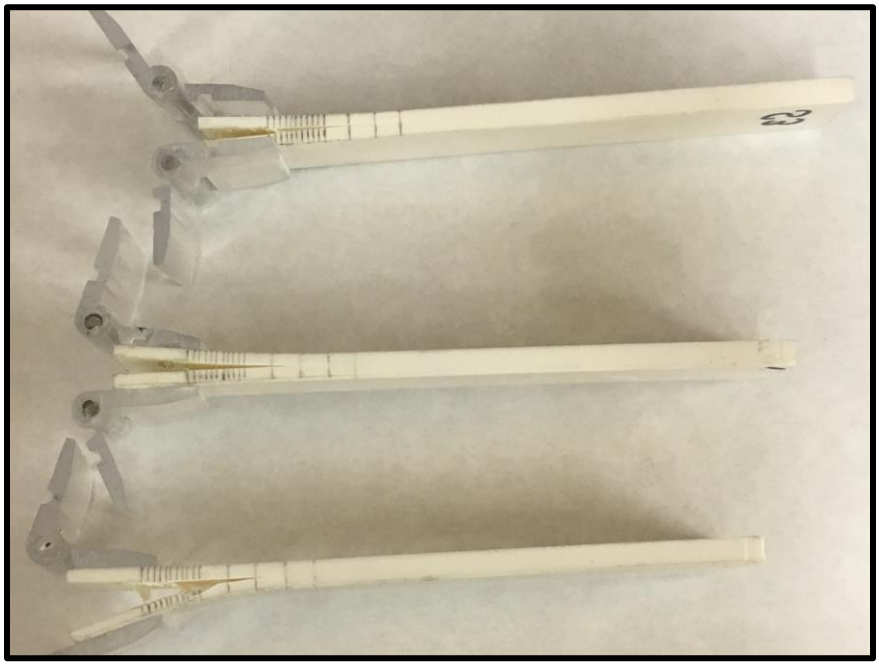

(a)

(b)

(c)

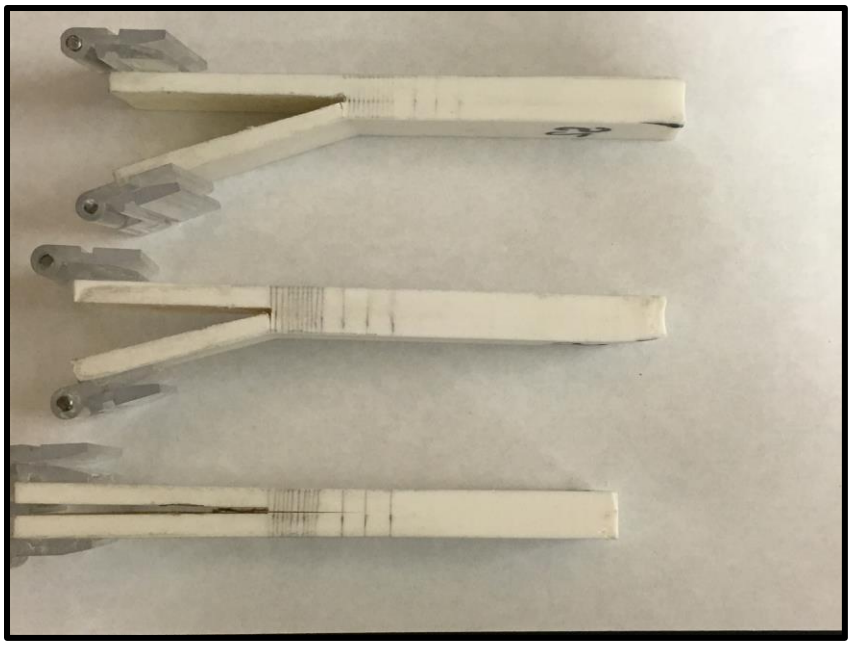

(d)

Figure 4-5 Crack propagation in specimen type

5A (a) 10A (b) 10B (c) and 10D (d)

(a)

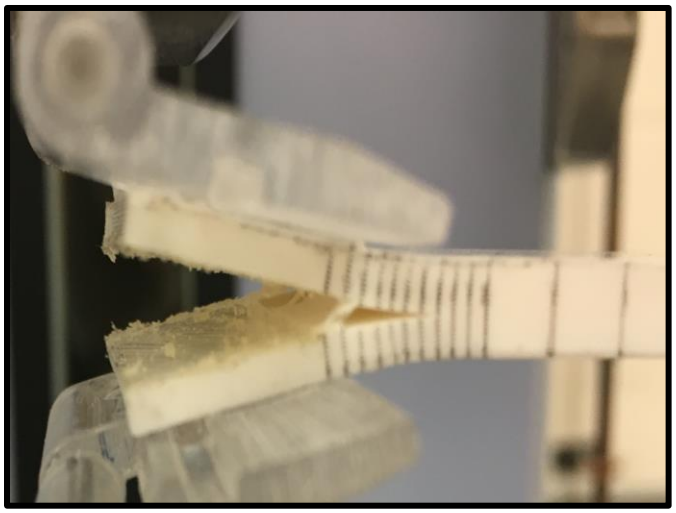

(b)

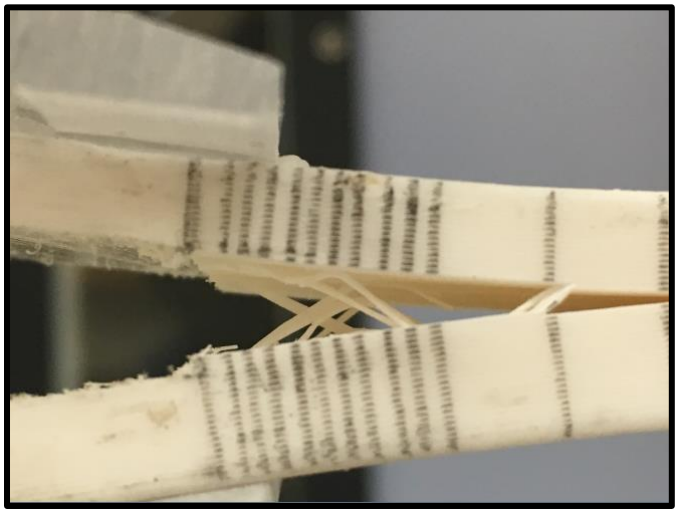

(c)

Figure 4-9 Crack propagation as observed in different specimens

4-5 Discussion

For all the cases studies, crack propagation was seen in some specimens. However, in other cases, the specimens either fractured at the load line or the hinges of

the specimens broke. The case studies can be compared based on three parameters – thickness of the specimens, initial crack length of the specimens, and initial crack diameter of the specimens. It appears from Fig. 4-9 that crack propagation is resisted via fiber bridging. This is most likely happening due to the location of initial crack being at the interior of the polymer material, not at the interfaces between rasters. As such, such events should be considered as experimental artifacts, not the general crack propagation mechanism during interlaminar fracture.

A. Thickness

For the 5A case, where the specimens are 5mm thick with initial crack length 12.06mm and crack diameter 0.25mm, crack propagation was observed in all the three cases. But for the 10A case, where the thickness was doubled leading to increase in geometrical thickness, it was observed that the hinges broke before the crack could be propagated. This lead to the understanding that on increasing the thickness, more load is required for the crack to propagate. This comparison study also showed that a better choice for the hinges could be used.

B. Crack Length

For the 10B specimens, the initial crack length was 12.06mm with initial crack diameter 0.76mm and specimen thickness 10mm, the crack was observed to propagate only in one out of three specimens. For the other two specimens, the hinges loosened.

For the case of 10D specimens with initial crack length of 50.8mm and other dimensions same as 10B, it was observed that crack propagated in one out of the three specimens. For the other two specimens however, the crack fractured at the load line.

C. Crack Diameter

In comparing the observations for 10A and 10B cases, the effect of variation in crack diameter was noted. It was observed that for 10A case, hinges broke and for 10B case, crack propagated only in one out of three specimens.

Chapter 5

Conclusion and Future Work

The classical lamination theory holds true for the straight bar laminate samples manufactured in the XYZ raster orientation as the results were coherent. Analysis of analytical data hence showed promising use of the classical lamination theory for failure prediction of tensile polymer specimens.

The static analysis data showed that with the use of correction factor of 0.79, the first ply failure load can be predicted within a 41N of difference from the load obtained from the maximum load corresponding to the linearity of the stress vs strain curves obtained from the experiments.

The double cantilever beam experiments showed that the propagation of crack depends on many factors such as initial crack thickness or diameter, initial crack length, and specimen thickness.

The proposed future work may include improving the analytical model of the classical lamination theory. This could be done by including the effects of curvature. This will allow us to study the mechanical behavior of the laminates with angled plies as well by creating a more general model. The analytical model can also be extended to study mechanical behavior of compression and shear loads. It also may be possible to study the hygroscopic and thermal effects using this model.

Computational study should be extended to fracture and flexural model. This will help establish a sound understanding for prediction of the fracture and flexural behavior.

More experiments should be done to analyze the effect of thickness and crack types. The choice of hinges can also be a parameter of study. Flexural experiments can also be performed to understand the fracture phenomenon more thoroughly.

References

[1] Zelinski, Peter (2014-06-25). "Video: World's largest additive metal manufacturing plant". Modern Machine Shop.

[2] "Print me a Stradivarius – How a new manufacturing technology will change the world". Economist Technology. 2011-02-10. Retrieved 2012-01-31.

[3] Sherman, Lilli Manolis. "3D Printers Lead Growth of Rapid Prototyping (Plastics Technology, August 2004)". Retrieved 2012-01-31.

[4] Anzalone, G.; Wijnen, B.; Pearce, Joshua M. (2015). "Multi-material additive and subtractive prosumer digital fabrication with a free and open-source convertible delta RepRap 3-D printer". Rapid Prototyping Journal. 21 (5): 506–519. doi:10.1108/RPJ-09-2014-0113.

[5] "3D printing: 3D printing scales up". The Economist. 2013-09-07. Retrieved 2013-10-30.

[6] Greenberg, Andy (2012-08-23). "'Wiki Weapon Project' Aims To Create A Gun Anyone Can 3D-Print At Home". Forbes. Retrieved 2012-08-27.

[7] Rayner, Alex (6 May 2013). "3D-printable guns are just the start, says Cody Wilson". The Guardian. London.

[8] "Cubify — Express Yourself in 3D". myrobotnation.com. Retrieved 2014-01-25.

[9] Wohlers Report 2009, State of the Industry Annual Worldwide Progress Report on Additive Manufacturing, Wohlers Associates, ISBN 978-0-9754429-5-1

[10] "Nokia backs 3D printing for mobile phone cases". BBC News Online. 2013-02-18. Retrieved 2013-02-20.

[11] Uta-ir.tdl.org. (2018). [online] Available at: https://uta-ir.tdl.org/uta-ir/bitstream/handle/10106/26440/KHATRI-THESIS-2016.pdf?sequence=1&isAllowed=y.

[12] Taufik M, Jain PK. A Study of Build Edge Profile for Prediction of Surface Roughness in Fused Deposition Modeling. ASME. *J. Manuf. Sci. Eng.* 2016;138(6):061002-061002-11. Doi:10.1115/1.4032193.

[13] Sung-Hoon, A., Montero, M., Odell, D., Roundy, S., & Wright, P. K. (2002). Anisotropic material properties of fused deposition modeling ABS. *Rapid Prototyping Journal, Vol. 8, Issue 4*, 248-257.

[14] Bellini, A., Guceri,S. (2003). Mechanical charaterization of parts fabricated suing fused deposition modeling. *Rapid Prototyping Journal, Vol 9, Issue 4*, 252-264.

[15] PolyPrinter. (2018). Rental - PolyPrinter 229. [online] Available at: http://www.polyprinter.com/rental-polyprinter-229/.

[16] Letcher, Todd & Rankouhi, Behzad & Javadpour, Sina. (2015). Experimental Study of Mechanical Properties of Additively Manufactured ABS Plastic as a Function of Layer Parameters. 10.1115/IMECE2015-52634.

[17] Goldberg, R. and Stouffer, D. (2002). Strain Rate Dependent Analysis of a Polymer Matrix Composite Utilizing a Micromechanics Approach. Journal of Composite Materials, 36(7), pp.773-793.

[18] Zou, R., Xia, Y., Liu, S., Hu, P., Hou, W., Hu, Q., & Shan, C. (2016). Isotropic and anisotropic elasticity and yielding of 3D printed material. Composites Part B:Engineering, 99, 506-513.

[19] Casavola, C., Cazzato, A., Moramarco, V., & Pappalettere, C. (2016). Orthotropic mechanical properties of fused deposition modelling parts described by classical laminate theory. Materials & Design, 90, 453-458.

[20] Bertoldi, M., Yardimci, M. A., Pistor, C. M., Guceri, S. I., & Sala, G. (1998). Mechanical characterization of parts processed via fused deposition. In Proceedings of the 1998 solid freeform fabrication symposium (pp. 557-565).

[21] Magalhães, L. C., Volpato, N., & Luersen, M. A. (2014). Evaluation of stiffness and strength in fused deposition sandwich specimens. Journal of the Brazilian Society Mechanical Sciences and Engineering, 36(3), 449-459.

[22] Alaimo, G., Marconi, S., Costato, L., & Auricchio, F. (2017). Influence of mesostructure and chemical composition on FDM 3D-printed parts. Composites Part B:Engineering, 113, 371-380.

[23] Aliheidari, N., Tripuraneni, R., Ameli, A., & Nadimpalli, S. (2017). Fracture resistance measurement of fused deposition modeling 3D printed polymers. *Polymer Testing*, *60*, 94-101.

[24] Patel, R., Shah, H. N., & Kumari, S. V. (2015). Experimental Investigation of Fracture of ABS Material by ASTM D-5045 for Different Crack Length & Layer of Orientation Using FDM Process. *Research Publish Journals, Volume 3, Issue 1*.

[25] Patel, N. D., & Patel, B. B. (2015). Fracture Analysis of FDM Manufactured Acryolnitrile Butadiene Styrene using FEM. *International Journal of Recent Research in Civil and Mechanical Engineering (IJRRCME). Vol 2, Issue 1*, 84-90.

[26] (2007). Fracture Mechanics Study of a Compact Tension Specimen. 3DS Simulia.

[27] Park, S. I., Rosen, D. W., Choi, S. K., & Duty, C. E. (2014). Effective mechanical properties of lattice material fabricated by material extrusion additive manufacturing. *Additive Manufacturing*, *1*, 12-23.

[28] Spoerk, M., Arbeiter, F., Cajner, H., Sapkota, J., & Holzer, C. (2017). Parametric optimization of intra-and inter-layer strengths in parts produced by extrusion-based additive manufacturing of poly (lactic acid). *Journal of Applied Polymer Science*, *134*(41).

[29] ASTM International. (2013). ASTM D5528-13 Standard Test Method for Mode I Interlaminar Fracture Toughness of Unidirectional Fiber-Reinforced Polymer Matrix Composites. https://doi.org/10.1520/D5528

[30] Hart, K. R., & Wetzel, E. D. (2017). Fracture behavior of additively manufactured acrylonitrile butadiene styrene (ABS) materials. *Engineering Fracture Mechanics*, *177*, 1-13.

[31] Chan, W. S. (2016, August). Chapter 2 Basic Concepts and Material characteristics. Arlington, Texas, United States of America.

[32] The Engineering Toolbox. (n.d.). Young's Modulus - Tensile and Yield Strength for common Materials. Retrieved from The Engineering Toolbox: https://www.engineeringtoolbox.com/young-modulus-d_417.html

[33] Anon, (2018). [online] Available at: https://www.researchgate.net/figure/a-Scheme-of-unidirectional-DCB-specimen-for-mode-I- test-b-DCB-specimen-of-different_fig4_258393201.

[34] Raney, J., Compton, B., Mueller, J., Ober, T., Shea, K. and Lewis, J. (2018). Rotational 3D printing of damage-tolerant composites with programmable mechanics. Proceedings of the National Academy of Sciences, 115(6), pp.1198-1203.

[35] craftunique.com. (2018). Craftunique - CraftBot Forum - View thread. [online] Available at: https://craftunique.com/forums/view-thread/273.

[36] Baikerikar, P. J., & Turner, C. J. (2017, August). Comparison of as-built FEA simulations and experimental results for additively manufactured dogbone geometries. In ASME 2017 International Design Engineering Technical Conferences and Computers and Information in Engineering Conference (pp. V001T02A021-V001T02A021). American Society of Mechanical Engineers.

Biographical Information

Megha Tangri pursued her Bachelors of Science in Aerospace Engineering from the University of Petroleum and Energy Studies, Dehradun, India. She pursued her Masters of Science in Mechanical Engineering from University of Texas at Arlington, US. Her research interest lies in Additive Manufacturing, composite materials, and polymers.